Research on the Signal Detection in an Uplink Ground-to-Satellite UDC-FSO System with Optical Path Difference

Ya-Tian Li[1], Zhi-Qiang Xu[1(✉)], Kai-Nan Yao[1,2], Rui-Peng Li[1,2], Lu Chen[1], and Hong-Zhuang Li[1]

[1] Changchun Institute of Optics, Fine Mechanics and Physics, Chinese Academy of Sciences, Changchun 130033, China
xuzhiqiang@ciomp.ac.cn
[2] University of Chinese Academy of Sciences, Beijing 100049, China

Abstract. This paper focuses on the optical path difference (OPD) in a 2×1 uplink ground-to-satellite free space optics (FSO) system with uniquely decodable codes (UDC), where the different data from transmitters (TXs) are superimposed asynchronously due to the OPD. We first analyze the influence of OPD on the uplink UDC-FSO system. Then the suboptimal minimal detection for moved patterns (MDMP) and optimal minimal metric-based pattern detection (MMPD) algorithms are proposed for mitigating the OPD-introduced interference, which are based on the minimum distance criterion and maximum likelihood sequence detection, respectively. Simulation results of symbol error rate (SER) and mutual information show that both of them outperform the case of directly detection notably. A desktop equivalent experiment is also built to verify the effectiveness of the proposed algorithms. It also promotes the potential for practical application of the UDC-FSO system.

Keywords: Free Space Optics · Uniquely Decodable Code · Optical Path Difference

1 Introduction

1.1 Background and Related Works

With the increasing demands for bandwidth and capacity, free space optics (FSO) has become a hot topic in the field of wireless communications, which

This work is supported by the National Natural Science Foundation of China (NO. 62101527).

H.-H. Chen and W. Meng (Eds.): WiSATS 2024, LNICST 605, pp. 89–101, 2025.
https://doi.org/10.1007/978-3-031-86196-3_8

has the advantages of easy placement, free of spectrum license, and small divergence angle to prevent interception [1,2]. Benefiting from these superiorities, FSO is widely used in ground-to-satellite links. Recently, the National Aeronautics and Space Administration (NASA) has conducted the Terabyte Infrared Delivery (TBIRD) program, achieving the burst rates up to 200 Gbps for optical communication links from low-Earth orbit to ground stations. This marks a new milestone in rate/throughput for point-to-point optical communications [3].

In further pursuit of higher data rates, different types of multiplexing techniques have been applied in FSO systems to improve throughput, such as using wavelength multiplexing [4], frequency multiplexing [5], angular momentum multiplexing [6], polarization multiplexing [7], and mode multiplexing [8]. The mentioned multiplexing techniques increase channel capacity by introducing additional parallel degrees of freedom. However, a single degree of freedom still has the potential to be exploited.

As a result, researchers invented the non-orthogonal multiple access (NOMA) techinique. Different from conventional orthogonal multiple access technique, NOMA technique enhances channel capacity by fully utilizing each degree of freedom [9]. NOMA technique can be categorized into power-domain (PD-NOMA) and code domain (CD-NOMA) according to the way of implementation. In the field of optical communications, PD-NOMA is primarily used for visible light communications (VLC), where the modulation method is always orthogonal frequency division multiplexing (OFDM) [10]. In FSO systems, which usually employ on-off keying (OOK) modulation, the transceiver structure and channel model are different from those in VLC. As a result, PD-NOMA is not commonly used in FSO.

On the basis that power signal superposition is mathematically consistent with code word superposition, CD-NOMA is an option for FSOs. Focusing on the area of CD-NOMA, our previous work [11–13] integrate the FSO and uniquely decodable codes (UDC) with the aim of leveraging the non-orthogonality of UDC to enhance channel capacity. We demonstrate that UDC codewords remain uniquely decodable (UD) even after passing through the fading channel in [11]. To quantitatively analyze the system performance, we deduce the theoretical value of the symbol error rate (SER) and calculate the channel capacity in [12]. Further, considering the multi-receiver scenario, two combination methods are proposed in [13], i.e., distance-based optimal candidate selection method and suboptimal maximization minimum distance combination method, both of which perform better than the traditional maximal ratio combining (MRC) method.

1.2 Motivation and Contribution

In our previous studies on UDC and FSO [11–13], it is assumed that the distances between all transmitters (TXs) and receiver (RX) are equal, which ensures synchronized superposition of the UDC codewords. However, in practice, especially in the ground-satellite uplinks, the optical path difference (OPD) is inevitable due to the fact that the satellite moves continuously while the ground stations are stationary, thus causing the signals from different TXs cannot be synchronized

superimposed on the RX [14,15]. Therefore, this paper focuses on a 2×1 uplink UDC-FSO scenario with OPD, aiming at designing signal detection algorithms to promote the practical application of UDC-FSO. The main contributions of this paper are illustrated as follows.

■ Different from the synchronous superposition cases, this paper investigates an asynchronous superposition scenario caused by the OPD between different TXs and RX.

■ We analyze the influence of OPD on the superimposed patterns in a uplink 2×1 UDC-FSO system.

■ To mitigate the interference, two signal detection algorithms are proposed, namely, the suboptimal minimal distance for moved patterns (MDMP) and optimal minimal metric-based pattern detection (MMPD).

■ By the simulations and experiments, the validity and feasibility of the proposed methods are verified by measuring the metrics such as the SER and the mutual information.

It is also worth noting that although both traditional optical code-division multiple-access (OCDMA) technique and UDC [16] are multiple access codes for FSOs, they are different. Since UDC is non-orthogonal and traditional OCDMA is always orthogonal. Another point that needs to be mentioned is that UDC is not a multi-decimal system, rather it can be constructed even under ternary or higher multi-decimal domains [17]. Moreover, common multiplexing techniques can be incorporated into the UDC-FSO system to further enhance channel capacity.

The structure of this paper is organized as follows. Section 2 briefly depicts the system model of a 2×1 uplink UDC-FSO links with OPD, as well as the channel model. Section 3.1 presents the influence of OPD on UDC-FSO. Section 3.2 and Sect. 3.3 cover the suboptimal MDMP and optimal MMPD algorithms, respectively. Section 4 shows the simulation results, while Sect. 5 illustrates the experimental ones. In the end, Sect. 6 concludes this paper.

2 System Model of a 2×1 Uplink UDC-FSO with OPD

2.1 System Structure and Influence of the OPD

This paper considers a 2×1 ground-to-satellite uplink UDC-FSO with OPD, where the UDC is utilized to allow the 2 TXs to transmit different data in a non-orthogonal way. For the sake of exposition, this paper considers a simple UDC codeword sets, i.e., $\mathbb{C}_1 = \{00, 01, 10\}$ and $\mathbb{C}_2 = \{00, 11\}$, respectively. According to [11], upper bounds on the amount of mutual information is equal to $\frac{1}{2}\log_2 6 = 1.2925$ bit/symbol (larger than 1 bit/symbol in the orthogonal case). The front coefficient 1/2 means that it takes 2 slots to transmit a UDC codeword. As shown in Fig. 1, baseband data $\mathbf{x_1}$ (or $\mathbf{x_2}$) in TX-1 (or TX-2) are first encoded into $\mathbf{c_1}$ or ($\mathbf{c_2}$) by UDC codeword sets, and then modulated and amplified. These signals out of the transmitting lens are further passing through the optical fading channels. Different from our previous works [11–13], where it's assumed that the UDC signals are superimposed synchronously at the RX, this

paper considers the case that there is a OPD between 2 uplinks. It's mentioned that we only need to consider the fractional part, due to the UDC codewords still maintain the UD feature after moving several integer codewords. Thus, this paper studies the case of fractional OPD and defines τ as the OPD of TX-1 to RX with respect to the TX-2 to RX link, satisfying $0 < \tau < 1$. Note that τ is a quantity in the time dimension, which has been normalized by the period time corresponding to the symbol clock rate. For the sake of analysis, it's also assumed that there is no frequency difference between the clocks at the TXs and RX, which can be reached by timing operation or timing recovery.

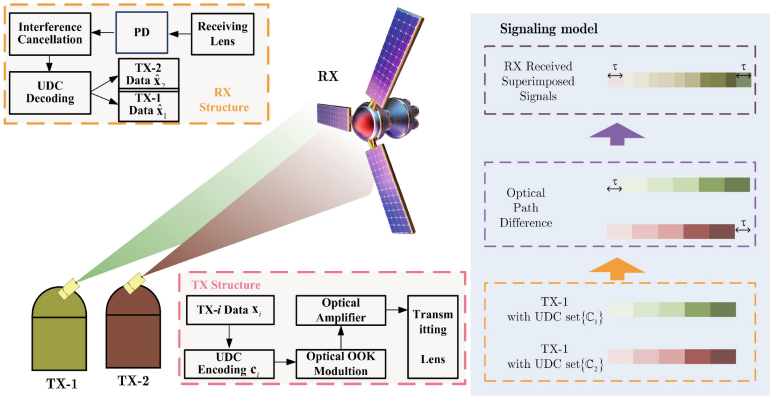

Fig. 1. System model of a 2 × 1uplink UDC-FSO with OPD.

From Fig. 1, the OPD τ cause interference to neighbor signals, and the received signals at RX (called as superimposed signals) can be expressed as

$$\mathbf{y}^k = \eta h_1^k \left[(1-\tau)\,\mathbf{c}_1^k(1) + \tau \mathbf{c}_1^k(2), (1-\tau)\,\mathbf{c}_1^k(2) + \tau \mathbf{c}_1^{k+1}(1)\right] + \eta h_2^k \mathbf{c}_2^k + \mathbf{n}_{\text{eq}}^k, \quad (1)$$

where the superscript k corresponds to k-th codeword. η stands for the photon-electric conversion ratio. $\mathbf{c}(1)$ (or $\mathbf{c}(2)$)is the first (or second) symbol in UDC codeword $\mathbf{c}$. $\mathbf{n}_{\text{eq}}^k$ represents equivalent Gaussian noise with the variance σ_n^2. It is worth mentioning that noted that the length of each vector in Eq. (1) is the exactly the same as the UDC codeword length. Due to the interference introduced by OPD, the RX tries to cancel the interference, and then decoding the UDC codewords from the superimposed symbols.

2.2 Channel Model

Considering link attenuation, Malaga turbulence and pointing errors [18], the probability distribution function (PDF) $f_h(h)$ of the channel gain h is shown below,

$$f_h(h) = \frac{\xi^2 A}{2h} \sum_{m=1}^{\beta} b_m \cdot \mathbf{G}_{1,3}^{3,0}\left[\frac{\alpha\beta}{(g\beta+\Omega')}\frac{h}{h_l A_0} \;\middle|\; \xi^2+1; \xi^2, \alpha, m\right], \quad (2)$$

where $\mathbf{G}_{p,q}^{m,n}(\cdot)$ is the Meijier'G function. α, β, g and Ω' are fading parameters of Malaga turbulence. A and b_m can be obtained from these parameters, by $\frac{2\alpha^{\alpha/2}}{g^{1+\alpha/2}\Gamma(\alpha)}(g\beta/g\beta+\Omega')^{\beta+\alpha/2}$ and $a_m[\alpha\beta/(g\beta+\Omega')]^{-(\alpha+m)/2}$, respectively. a_m denotes $\left(\frac{\beta-1}{m-1}\right)\left(g\beta+\Omega^{'}\right)^{1-m/2}/(m-1)!\left(\Omega^{'}/g\right)^{m-1}(\alpha/\beta)^{m/2}$. Both A_0 and ξ means the pointing error parameters. Specifically, A_0 defines the pointing loss, while ξ is the ratio between the receiver's equivalent beam radius and pointing error displacement standard deviation.

3 Signal Detection Algorithms for UDC-FSO with OPD

In this section, the influence of OPD τ is first discussed. Then the suboptimal and optimal algorithms for signal detection are illustrated, respectively.

3.1 Influence of OPD on UDC-FSO

Before discussing the OPD on UDC-FSO, we need to review the definition of superimposed patterns. The superimposed patterns are the superimposed UDC codewords after fading channels, i.e., $\eta h_1^k \mathbf{c}_1^k + \eta h_2^k \mathbf{c}_2^k$ in the ideal UDC-FSO case, where there are $2 \times 3 = 6$ superimposed patterns (labeled as $\varphi_1, ..., \varphi_6$) as shown in the first line of Fig. 2. It can be also defined that φ^k is the corresponding k-th superimposed pattern in the ideal UDC-FSO without OPD. The UD characteristic of UDC ensures that the superimposed pattern corresponds one-to-one with the UDC codewords from TXs. This means that the receiver can still recover the original data from the superimposed signals.

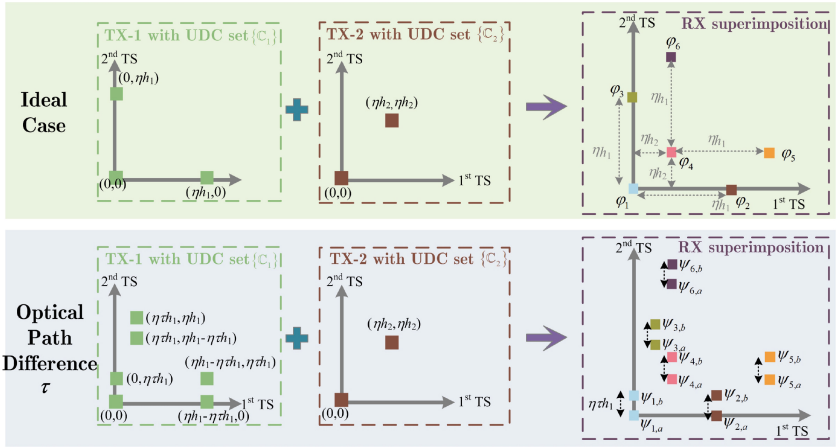

Fig. 2. The influence of OPD on superimposed patterns of UDC-FSO systems.

Under the circumstances of OPD $0 < \tau < 1$, the part τ of the first symbol in each superimposed pattern contributes to the previous superimposed pattern. So

does the next superimposed patterns. The moved superimposed patterns can be defined as $\eta h_1^k \left[(1-\tau)\,\mathbf{c}_1^k(1)+\tau\mathbf{c}_1^k(2),(1-\tau)\,\mathbf{c}_1^k(2)+\tau\mathbf{c}_1^{k+1}(1)\right]+\eta h_2^k\mathbf{c}_2^k$. Due to the fact of $\mathbf{c}_1^{k+1}(1)=0$ or 1, the number of superimposed patterns has doubled. For ease of presentation, $\psi_{i,a}$ (or $\psi_{i,b}$) represents the changed superimposed patterns with the subsequent codeword starting with symbol "0" (or "1"), as given in Fig. 2's second line. It shows how the superimposed patterns will be changed when there is OPD. It's apparent that the locations of superimposed symbol have moved, where distance between these superimposed patterns is also shortened. It will certainly result in poorer SER and mutual information.

However, the changed superimposed patterns can still be categorized into 6 parts (defined as $\boldsymbol{\psi}_i=\{\psi_{i,a},\psi_{i,b}\}, i=1,\ldots,6$), which are also corresponding to the original ideal superimposed patterns. We also define the operation $\mathcal{D}[\bullet]$ to be the mapping from moved superimposed pattern $\psi_{i,j}$ to original superimposed pattern and next codeword $\mathbf{c}_1^{k+1}$,i.e., $\psi_{i,j}=\mathcal{D}\left(\varphi^k,\mathbf{c}_1^{k+1}\right)$. The mapping relationship is summarized in Table 1.

Table 1. Superimposed patterns after OPD

$\psi_{i,j}=\mathcal{D}\left(\varphi^k,\mathbf{c}_1^{k+1}\right)$	$\mathbf{c}_{k+1}=[0,0]$ or $[0,1]$ $(\varphi^{k+1}=\varphi_1,\varphi_3,\varphi_4,\varphi_6)$	$\mathbf{c}_{k+1}=[1,0]$ $(\varphi^{k+1}=\varphi_2,\varphi_5)$
$\varphi^k=[0,0]$	$\psi_{1,a}=[0,0]$	$\psi_{1,b}=[0,\eta\tau h_1]$
$\varphi^k=[\eta h_1,0]$	$\psi_{2,a}=[\eta h_1(1-\tau),0]$	$\psi_{2,b}=[\eta h_1(1-\tau),\eta\tau h_1]$
$\varphi^k=[0,\eta h_1]$	$\psi_{3,a}=[\eta\tau h_1,\eta h_1(1-\tau)]$	$\psi_{3,b}=[\eta\tau h_1,\eta h_1]$
$\varphi^k=[\eta h_2,\eta h_2]$	$\psi_{4,a}=[\eta h_2,\eta h_2]$	$\psi_{4,b}=[\eta h_2,\eta h_2+\eta\tau h_1]$
$\varphi^k=[\eta h_1+\eta h_2,\eta h_2]$	$\psi_{5,a}=[\eta h_1(1-\tau)+\eta h_2,\eta h_2]$	$\psi_{5,b}=[\eta h_1(1-\tau)+\eta h_2,\eta h_2+\eta\tau h_1]$
$\varphi^k=[\eta h_2,\eta h_1+\eta h_2]$	$\psi_{6,a}=[\eta h_2+\eta\tau h_1,\eta h_1+\eta h_2-\eta\tau h_1]$	$\psi_{6,b}=[\eta h_2+\eta\tau h_1,\eta h_1+\eta h_2]$

3.2 Suboptimal MDMP Algorithm

In order to detection the symbols, this paper supposes that the RX has the ability of estimating the OPD τ, where the estimation may be achieved with maximum likelihood estimation [15]. With available OPD τ, an intuitive idea is to utilize maximum likelihood methods for detection. Therefore, we design the algorithm named as MDMP. The present challenge is how to adjudicate the 12 kinds of received signals into the 6 original superimposed patterns. Therefore, we first calculate current 12 superimposed patterns, and judge the received superimposed signal $\mathbf{y}$ into the potential superimposed patterns according to the minimum distance criterion.

$$\hat{\psi}_{i,j}=\arg\min_{i,j}\left|\mathbf{y}-\psi_{i,j}\right|, i=1,...,6; j=a \text{ or } b. \tag{3}$$

Then we correspond the obtained $\hat{\psi}_{i,j}$ to the ideal superimposed pattern ψ_i by Table 1. The data can be further decoded by regular UDC decoders [11–13].

3.3 Optimal MMPD Algorithm

As mentioned above, the suboptimal MDMP algorithm considers the moved superimposed pattern. However, the effect of each judged codeword on neighboring codewords is not fully utilized. Thus we propose the MMPD algorithm based on maximum likelihood sequence detection. Given the one-to-one correspondence between the UDC and the original data $\mathbf{x}_k$, the $\hat{\mathbf{x}}_k$ can be obtained by adjudicating the correct superimposed pattern.

$$\hat{\varphi}^k = \arg\max_{\varphi^k} \sum_{k=1} \ln\left[P\left(\mathbf{y}^k \mid \varphi^k, \mathbf{c}_1^{k+1}, \tau\right)\right], \tag{4}$$

where $P\left(\mathbf{y}^k \mid \varphi^k, \mathbf{c}_1^{k+1}, \tau\right)$ is the conditional PDF, given as

$$P\left(\mathbf{y}^k \mid \varphi^k, \mathbf{c}_1^{k+1}, \tau\right) = \frac{1}{\sqrt{2\pi}\sigma_n} \exp\left[-\frac{1}{2\sigma_n^2} \cdot \left|\mathbf{y}^k - \psi_{i,j}^k\right|^2\right], \psi_{i,j} = \mathcal{D}\left(\varphi^k, \mathbf{c}_1^{k+1}\right). \tag{5}$$

By substituting Eq. (5) to Eq. (4),

$$\hat{\varphi}_i^k = \arg\min_{\varphi_i^k} \sum_{k=1} \left|\mathbf{y}^k - \psi_{i,j}\right|^2, \psi_{i,j} = \mathcal{D}\left(\varphi^k, \mathbf{c}_1^{k+1}\right). \tag{6}$$

Table 2. Pseudo-code diagram of the MMPD algorithm

Input:$\{\mathbf{y}_k\}$, h_1^k, h_1^k τ (k=1,2,,N_c).
Output:Detected signals $\hat{\mathbf{x}}_1^k$ and $\hat{\mathbf{x}}_2^k$.

Initialize $\mathcal{A}_p = \infty$ for p =2,6, $\mathcal{A}_p = 1$, $\mathcal{R}$ = zeros $(6, N_c)$, $\mathcal{B}_p = \infty$ for $p = 1, 2, , 6$.
FOR $k = 1 : N_c$
  FOR $p = 1 : 6$, $q = 1 : 6$
    Calculate current distance $\mu_{p,q} = \left|\mathbf{y}^k - \psi_{p,j}^k\right|, j = a$ (q = 2,5), $j = b$ ($q = 1, 3, 4, 6$).
    IF $\mathcal{B}_p > \mathcal{A}_p + \mu_{p,q}$
      Update the current distance value by $\mathcal{B}_p = \mathcal{A}_p + \mu_{p,q}$.
      Record the current path node $\mathcal{R}_q^k = p$.
    END IF
  END FOR
  Update cumulative distance $\mathcal{A}_p = \mathcal{B}_p$ for $p = 1, , 6$.
END FOR
Find $p = \arg\min_p \{\mathcal{A}_p\}$.
FOR $k = N_c$: -1: 1
  Obtain the judged superimposed patterns $\hat{\varphi}_i^k = \mathcal{R}_p^k$.
  Update the index $p = \mathcal{R}_p^k$.
End FOR
Decode from ideal UDC superimposed patterns $\hat{\varphi}_i^k$ to $\hat{\mathbf{x}}_1^k$ and $\hat{\mathbf{x}}_2^k$ for $k = 1, , N_c$.

By observing the form of Eq. (6), it is equivalent to minimizing the sum of distances between the superimposed signal $\mathbf{y}^k$ and the superimposed patterns $\psi_{i,j}^k$. In other words, the key merit is the summation of the distances. Therefore, we can model the MMPD algorithm after the Viterbi method by recording lattice graph paths. Each step in the lattice graph has six nodes, and each node corresponds to a kind of superposition pattern. Due to the uniformity and traversal of the code word, each node has 6 possible paths.

We Define $\mathcal{A}_p$ to represent the previous cumulative distance on the p-th node. Similarly we define $\mathcal{B}_p$ to be the current cumulative distance value on the p-th node. Also the register $\mathcal{R}_p^k$ $(p = 1, \ldots, 6; k = 1, \ldots, N_c)$ represents the stacked node number corresponding to ψ_p in the k-th transmission codeword. The pseudo-code diagram is shown in Table 2, where N_c denotes the number of transmitted codewords in each TX. For ease of representation, we may suppose that the first codeword sent to be [0,0] for both TXs, i.e., $\psi^{k=1} = \psi_1$.

4 Simulation Results

Simulations of a 2×1 uplink UDC-FSO with OPD are carried out in this section. The simulation parameters are summarized in Table 3. It is also important to mention here that unlike conventional RF communication systems, the signal-to-noise ratio (SNR) is proportional to the transmit power. In intensity-modulated/direct-detection (IM/DD) FSO systems, the SNR will be proportional to the square of the transmit power [19]. Therefore, SNR from 0 to 50 dB is a suitable range.

Table 3. Simulation Parameters

Parameters	Values
Link distance	4000 km
Beam Divergence Angle	30 μrad
Malaga Turbulence	$(\alpha, \beta, g, \Omega') = (8, 4, 0.02, 1)$
Pointing Errors	$A_0 = 1$, $\xi = 6.7$
OPD	$\tau = 0.2$

Figure 3 depicts the SER of a 2×1 uplink UDC-FSO system with OPD $\tau = 0.2$, as well as the mutual information. It's found that both the MDMP and MMPD algorithms outperform the direct detection (unknown τ, as a control group). The optimal MMPD can approach the ideal UDC-FSO without OPD in case of high SNR, while the suboptimal MDMP still has a gap with the ideal UDC-FSO even though the SNR is high enough. It's obtained that the slopes of the SERs of MDMP, MMPD, ideal UDC-FSO and the ideal point-to-point (P2P) FSO case are almost the same when τ is equal to 0.2, which indicates that they have almost the same diversity order of 1. This is easy to understand

since the employment of UDC in 2×1 links is to apply its CD-NOMA property, where the TXs send different messages with no diversity gain. In addition, the direct detection with unknown τ has an error floor in the SER curve, which owes to the OPD's interference to neighbor superimposed patterns. As can be also found from Fig. 3(b), the mutual information of UDC-FSO with OPD τ can still approach the upper bound of ideal UDC-FSO systems, i.e. $\frac{1}{2}\log_2 6 = 1.2925$ bit/symbol, when the MDMP or MMPD are employed. It's implied that the effectiveness of the proposed algorithms.

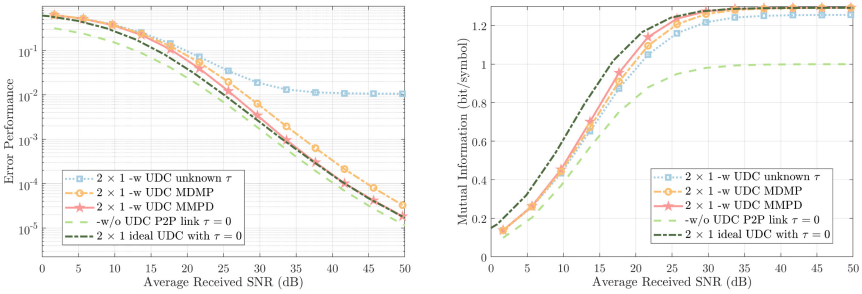

(a) SER (b) Mutual Information

Fig. 3. Simulation Performance of different algorithms with $\tau = 0.2$.

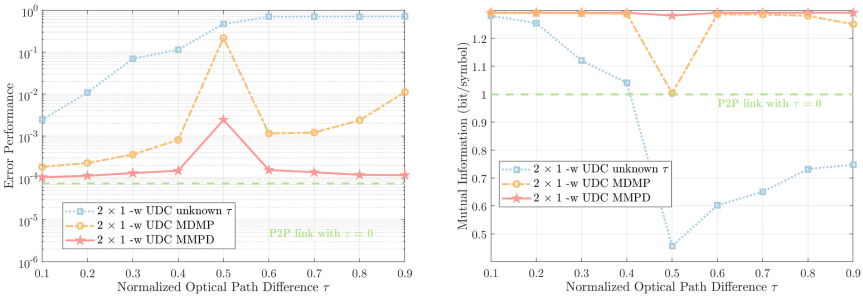

(a) SER (b) Mutual Information

Fig. 4. Simulation performance versus different τ.

Considering that Fig. 3 only considers the case when $\tau = 0.2$, we explore the performance of the UDC-FSO system for different OPD τ in Fig. 4. Similar to Fig. 3, the curves of SER and mutual information are represented in Figs. 4(a) and 4(b), respectively. It's seen that the gap between optimal MMPD and suboptimal MDMP becomes larger with increasing OPD τ. Specifically, for the SER metric, the suboptimal MDMP performs barely acceptably when the OPD τ is

less than 0.4, while the optimal MMPD consistently exhibits excellent performance and is close to the traditional P2P case. From both Figs. 4(a) and 4(b), it can be found that OPD $\tau = 0.5$ is the worst case, because under this condition, superimposed patterns $\psi_{2,b}$ and $\psi_{3,a}$ will overlap, so will $\psi_{5,b}$ and $\psi_{6,a}$. Misclassification will often occur leading to performance degradation. This also implies why the MMPD performance is positively correlated with $|\tau - 0.5|$ for the same SNR.

5 Experimental Results

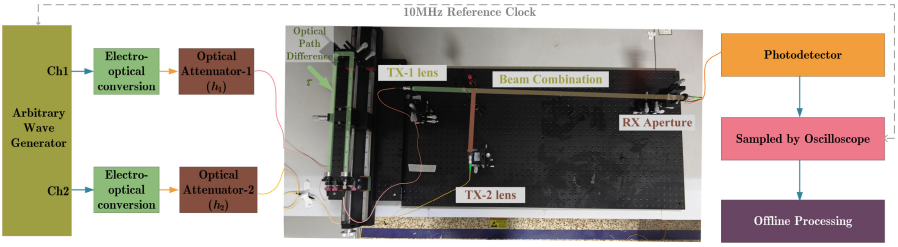

Fig. 5. Experiment scene of a desktop equivalent 2×1UDC-FSO system with OPD.

After simulations analysis, a 2×1 UDC-FSO equivalent desktop experiment is built, as shown in Fig. 5. Two homologous channels of the Arbitrary Wave Generator (AWG, Tektronix AWG70002A) produce the UDC-encoded electrical signals which are further modulated by the electro-optical modulator. There is an optical attenuator in each TX where the attenuation values consist of the path loss and channel fading introduced by turbulence and pointing errors. By adjusting the optical attenuator and the transmitting power, it makes the desktop experiment similar as the slant ground-to-satellite link. It's also noted that the OPD is achieved by a linear guideway, where the optical beam in TX-1 enters a collimator after passing through one transmitting lens and two 45-degree mirrors. The OPD is set to be 67.5 cm, i.e., $\tau = 0.45$ for symbol rate of 200 MHz. The signals from 2 TXs are combined and then coupled into a multimode fiber at the RX, which are converted to electrical signals. These electrical signals are further sampled and stored by an oscilloscope (Tektronix, DPO7354). The AWG also provides a 10 MHz reference clock for the oscilloscope to ensure that there is no frequency difference between the TXs and RX. The collected data are first transmitted to a computer and further processed in an offline way.

The experimental results are shown in Fig. 6. As can be seen from Fig. 6(a), the number of superimposed signals has doubled, compared to the case of no OPD, which is consistent with the analysis in Fig. 2. Figure 6(b) provides both the SER and mutual information of optimal MMPD and suboptimal MDMP algorithms, where the direct detection with unknown τ is also depicted. We

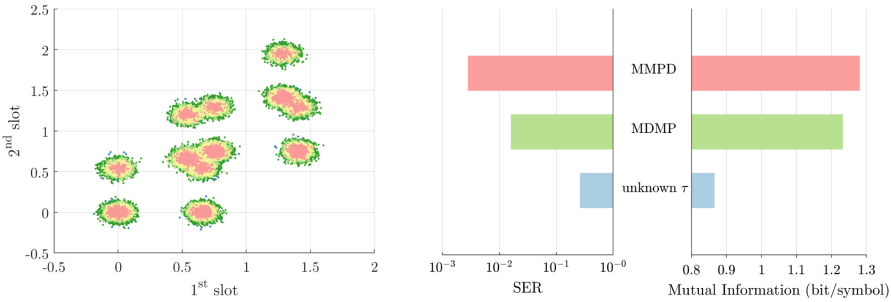

(a) Superimposed signals (b) Performance of detection methods

Fig. 6. Experimental Results of UDC-FSO with OPD.

can obtain similar conclusions to the simulations that the proposed MMPD and MDMP methods can both mitigate the interference introduced by the OPD τ. The mutual information after optimal MMPD is close the upper bound of ideal UDC-FSO systems. Additionally, the experiments also imply that the proposed algorithms can enhance the tolerability of the UDC-FSO system for real asynchronous situations, thus increasing its potential for application in real systems.

6 Conclusion

Our previous works have verified the feasibility of UDC-FSO systems, whose main advantage is to allow TXs to transmit different data in a CD-NOMA way. This paper considers an actual scene of a 2×1 ground-to-satellite UDC-FSO link, where there is an OPD between the 2 uplinks. It's discovered that the OPD not only doubles the number of superimposed patterns, but also shifts the locations of the superimposed patterns. Consequently, the minimum distance between the superimposed patterns becomes smaller, thus degrading the system SER and the amount of mutual information. In order to more accurately detect the signals with interference, this paper proposes the suboptimal MDMP and optimal MMPD algorithms, which are based on the minimum distance criterion and maximum likelihood sequence detection, respectively. Both simulation and experimental results show that the SER and mutual information by the proposed algorithms outperform the traditional direct detection method. Specifically speaking, the optimal MDMP can approach the ideal UDC-FSO case in case of high SNR, while the suboptimal MDMP still has a gap compared with the optimal MDMP even in the high SNR case. The suboptimal MDMP is bearable with $\tau < 0.4$. The gap between the suboptimal MDMP and optimal MMPD becomes larger with increasing OPD τ. Besides, it's also found the worst situation is the OPD $\tau = 0.5$ for all the mentioned algorithms, owing to the overlap of superimposed patterns $\psi_{2,b}$ and $\psi_{3,a}$ (also $\psi_{5,b}$ and $\psi_{6,a}$). Overall, this paper serves as a starting point and enhances the possibility of applying the UDC-FSO system in practical scenarios. Subsequent works may focus on further

investigation in scenarios where there are clock frequency differences between the transceivers or non-perfect estimation of the OPD.

References

1. Jahid, A., Alsharif, M.H., Hall, T.J.: A contemporary survey on free space optical communication: potentials, technical challenges, recent advances and research direction. J. Netw. Comput. Appl. **200**, 103311 (2022)
2. Karmous, S., Adem, N., Atiquzzaman, M., Samarakoon, S.: How can optical communications shape the future of deep space communications? A Survey. IEEE Commun. Surv. Tutor. 1 (2024). https://doi.org/10.1109/COMST.2024.3403873.
3. Schieler, C M., et al.: 200 Gbps TBIRD CubeSat downlink: pre-flight test results. In: Hemmati, H., Robinson, B.S. (eds.) Free-Space Laser Communications XXXIV, 119930P, SPIE (2022)
4. Fadil, E.A., Abass, A.K., Tahhan, S.R.: Secure WDM-free space optical communication system based optical chaotic. Opt. Quantum Electron. **54**(8), 477 (2022)
5. Ahmed, M.S., Gucluoglu, T.: Maximum ratio transmission based generalized frequency division multiplexing over gamma-gamma channel. Opt. Commun. **492**, 126965 (2021)
6. Zhao, L., et al.: High-accuracy mode recognition method in orbital angular momentum optical communication system. Chin. Opt. Lett. **20**(2), 020601 (2022)
7. Singh, M., Aly, M.H., El-Mottaleb, S.A.A.: Performance analysis of a 448 GBPS PDM/WDM/16-QAM hybrid SMF/FSO system for last mile connectivity. Opt. Quantum Electron. **55**(3), 231 (2023)
8. Kakati, D., Minz, M., Sonkar, R.K.: Performance analysis of grating-assisted passive mode-division multiplexing device using silicon photonics for high-speed RoF/RoFSO communication. Opt. Eng. **60**(1), 016102 (2021)
9. Liu, Y., et al.: Evolution of NOMA toward next generation multiple access (NGMA) for 6G. IEEE J. Sel. Areas Commun. **40**(4), 1037–1071 (2022)
10. Vappangi, S., Deepa, T., Mani, V.V., Bharathiraja, N.: On the performance of delta sigma modulators for DCO-OFDM based NOMA visible light communication systems. Opt. Laser Technol. **167**, 109653 (2023)
11. Li, Y., Geng, T., Gao, S.: Improve the throughput of M-to-1 free-space optical systems by employing uniquely decodable codes. Chin. Opt. Lett. **21**(3), 030603 (2023)
12. Li, Y., Geng, T., Gao, S.: On the error performance and channel capacity of a uniquely decodable coded FSO system over Malaga turbulence with pointing errors. Opt. Express **31**(21), 34264–34279 (2023)
13. Li, Y., Geng, T., Gao, S.: On the signal combinations for a uniquely decodable coded MIMO-FSO communication system. Opt. Laser Technol. **172**, 110533 (2024)
14. Liu, Y., He, Y., Chen, K., Guo, L.: Asynchronous transmission for cooperative free-space optical communication system. IEEE Wirel. Commun. Lett. **11**(4), 766–770 (2022)
15. Li, Y., Geng, T., Gao, S.: Likelihood based synchronization algorithms in optical pulse position modulation systems with photon-counting receivers. Opt. Express **30**(17), 31472–31485 (2022)
16. Hacini, L., Aissaoui, A.: Performance evaluation of SAC-OCDMA-FSO system based on LSC code under fog conditions. Opt. Quantum Electron **55**(2), 189 (2023)

17. Lu, S., Hou, W., Cheng, J., Kamabe, H.: Recursive construction of k-ary uniquely decodable codes for multiple-access adder channel. In: 2018 International Symposium on Information Theory and Its Applications, pp. 565–569, Singapore. IEEE (2018)
18. Ansari, I.S., Yilmaz, F., Alouini, M.-S.: Performance analysis of free-space optical links over Malaga (M) turbulence channels with pointing errors. IEEE Trans. Wireless Commun. **15**(1), 91–102 (2016)
19. Uysal, M., Capsoni, C., Ghassemlooy, Z., Boucouvalas, A., Udvary, E.: Optical Wireless Communications: An Emerging Technology. Springer, Cham (2016)